



The effect of equivalence ratio on the soot onset chemistry in one-dimensional, atmospheric-pressure, premixed ethylbenzene flames

Ali Ergut^a, Yiannis A. Levendis^{a,*}, Henning Richter^b, Jack B. Howard^b,
Joel Carlson^c

^a *Mechanical and Industrial Engineering, Northeastern University, Boston, MA 02115, USA*

^b *Chemical Engineering, Massachusetts Institute of Technology, Cambridge, MA 02139, USA*

^c *US Army SBCCOM—Natick Soldier Center, Natick, MA 01760, USA*

Received 22 September 2006; received in revised form 20 February 2007; accepted 19 April 2007

Available online 11 June 2007

Abstract

An investigation was conducted on the evolution of products of incomplete combustion (PIC) emitted from one-dimensional, laminar, atmospheric-pressure ethylbenzene flames in the vicinity of the soot onset threshold. The objective of this study was to identify the role of the fuel-to-air equivalence ratio in the evolution of polycyclic aromatic hydrocarbons (PAH) and other PIC as soot precursors, just prior to and subsequent to soot onset in premixed flames. Liquid ethylbenzene was prevaporized in nitrogen and blended with an oxygen–nitrogen mixture. Upon ignition, premixed flat flames were stabilized over a burner at atmospheric pressure. Temperature measurements and product sampling were conducted at various heights above the burner. Collected samples were analyzed for soot, PAH, oxygenated species, fixed gases, and light hydrocarbons. Three flames were investigated in the vicinity of the observed soot onset threshold, at equivalence ratios of $\phi_1 = 1.68$, $\phi_2 = 1.74$, and $\phi_3 = 1.83$. By adjusting the amounts of oxygen, nitrogen, and fuel, both the maximum measured flame temperature and the spatial profile of the temperature were kept nearly constant as the equivalence ratio was varied. The cold gas velocity through the burner was also kept nearly constant. Changes in species concentration profiles prior to, at and beyond the sooting limit were evaluated. The results indicated that the soot onset limit is not a function of flame temperature alone; i.e., while the maximum measured flame temperatures was kept fairly constant, the flame could be either sooting, at the sooting limit or nonsooting depending on the equivalence ratio. A detailed chemical kinetic model, previously tested against sooting premixed benzene and ethylbenzene flames, was used to gain insight in chemical processes involved in soot formation. A reaction flux analysis was conducted to determine the pathways for ethylbenzene consumption, as well as for benzene and naphthalene formation. Examination of experimental measurements of species along the axis of the flame, in view of the theoretical predictions, showed a rather direct correlation of acetylene to soot formation. Moreover, a correlation between the consumption of ethylbenzene pyrolyzates, such as styrene, and soot formation at the soot onset was also apparent. Whereas the model's results were very encouraging, additional development is deemed necessary to improve its predictive capability in the challenging regime of soot inception.

*

© 2007 The Combustion Institute. Published by Elsevier Inc. All rights reserved.

Keywords: Equivalence ratio; PAH; Ethylbenzene; Premixed flames; Soot onset

1. Introduction

Consumption of gasoline and other oil products is growing around the world. Global petroleum demand grew by 3.2% in 2004, 1.3% in 2005, and 1.01% in 2006. Another 1.85% growth is expected in 2007 as demand rebounds in the United States and China [1–3]. Gasoline is a mixture of saturated aliphatic hydrocarbons (C_nH_{2n+2}) in the C_6 – C_{10} range, aromatic compounds (Benzene, Toluene, Ethylbenzene, and Xylene—BTEX), and oxygenated species (such as methyl tertiary-butyl ether (MTBE) and ethanol). Aromatic compounds are desirable in gasoline since they increase the octane number rating of the fuel, and hence they allow higher compression ratios, r_c , and therefore higher engine efficiency (the theoretical Otto cycle efficiency is $\eta = 1 - r_c^{(1-\gamma)}$, where γ is the ratio of specific heats c_p/c_v).

Ethylbenzene (C_8H_{10}) is an important aromatic component of gasoline blends with weight fractions on the order of 0.2–4% [4–7]; it is also present in smaller quantities in other fuels, such as diesel oil, jet-A, JP-8, etc., as well as in inks, paints, and insecticides, which are often incinerated at the end of their life cycles. In 2006 around 142 billion gallons of gasoline was consumed in United States alone. Assuming an average of 2 wt% ethylbenzene content, this corresponds to 9.3 million tons of ethylbenzene burned in gasoline engines. Although combustion mostly occurs under stoichiometric conditions in conventional spark-ignited gasoline engines, new technologies, such as direct injection spark-ignited engines, necessitate better understanding of combustion characteristics of fuel components under locally fuel-rich conditions. Ethylbenzene is also burned, although in lesser amounts, in diesel engines and aeroturbines, being a minor component of diesel oil and aviation fuel.

It is important to understand the combustion characteristics of the aromatic compounds in gasoline, since they have a higher propensity to form PAH and soot as compared to aliphatic compounds [8,9]. While most of the PAH do not show mutational activity, some are known carcinogens and a large number have been shown to cause mutations of single cells, both bacterial and human. Especially benzo(a)pyrene, fluoranthene, and cyclopenta[cd]pyrene are combustion products, which are mutagenic. Cyclopenta[cd]pyrene is very active in human lung cells [10].

Additionally, ethylbenzene has been reported to convert to styrene (C_8H_8) extensively and extremely fast [11]. Since polystyrene ($(C_8H_8)_n$) also converts primarily to styrene (~75%) [12], it may be considered as a surrogate for polystyrene combustion as well. Thus, this investigation also relates to past work in this laboratory on the combustion and emissions of waste polystyrene (PS), styrene, and ethylbenzene [13–28]. Combustion of polystyrene (PS), which amounts to 22 wt% of all high-volume waste plastics [29], generates larger amounts of polycyclic aromatic hydrocarbons (PAH) and soot than other plastics. This is attributed to its aromatic structure [13–15].

To minimize emissions from combustion sources, a good understanding of the factors governing the propensity to form soot is required. Some fuels are sootier than others; i.e., the fuel molecular structure, along with flame temperature, fuel/oxidizer ratio, gas dynamics of the system, and pressure, is an influential parameter that determines the threshold and quantity of soot formed in a given flame.

There are two distinct facets to the effects of the fuel molecular structure on sooting propensity. First, as a given premixed fuel/oxidant combination is made increasingly fuel-rich, a rather sharp onset of sooting is observed. This facet of the tendency to soot is important in practical applications where total absence of sooting is desirable. The second facet is that further increasing the fuel concentration beyond the point of soot onset causes increasingly greater quantities of soot to form at a rate, which depends on fuel structure.

The most widely discussed aspect of molecular structure effects on soot threshold is the general ranking of sooting tendencies. Based on data obtained from flames on a Bunsen burner, Street and Thomas, in a pioneer investigation [8] reported that the sooting tendencies of hydrocarbons rank as acetylene < alkenes < isoalkanes < *n*-alkanes < alkylbenzenes < naphthalenes. It is important to note, though, that in burner-type combustion systems it is difficult to separate the effect of the equivalence ratio from that of the temperature, since temperature is also a function of equivalence ratio. The present work attempts to decouple the effects of these two parameters.

Takahashi and Glassman [30] concluded that sooting limits in premixed flames arise from a competition between fuel pyrolysis and oxidative attack. They correlated the sooting limits of premixed flames for a wide range of fuels by accounting for C–C bonds and flame temperatures, and found that the structure of

the fuel molecule was not important. All fuels break down to the same essential species, such as acetylene, which build into soot. Thus, fuel pyrolysis controls the sooting tendency. However, in the case of aromatic fuels, an additional fast and direct route may produce soot through condensation of aromatic rings into graphite-like structures, particularly at temperatures below 1800 K [31–33]. Markatou et al. [34] performed detailed kinetic calculations to validate the soot formation mechanism and postulated that oxidation of light pre-aromatic-ring species, such as C_2H_3 , may be even more important than oxidation of PAH for defining sooting limits in *premixed* flames. Sooting limits provide rigorous tests of the accuracy of soot-particle inception models because they involve PAH chemistry [35] isolated from physical phenomena such as condensation/coagulation/agglomeration of particles.

The formation of particulate matter in fuel-rich combustion is typically modeled through the formation of small aromatic species, such as benzene, that grow to high-molecular-mass aromatics including PAH. However, most flame studies of soot formation chemistry have used methane, ethylene, or acetylene as the fuel. These C_1 – C_2 fuels lack most of the structural features that are characteristic of liquid-fuel hydrocarbons: alkyl carbon–carbon bonds, alkyl rings, allylic bonds, and benzenoid rings. Thus their flames provide an incomplete picture of fuel decomposition and aromatics formation chemistry. A recent, detailed review on the combustion chemistry of larger, more complex hydrocarbons investigated the effects of these characteristic structures on the fuel decomposition and aromatic formation chemistry [36]. The general, widely accepted, picture of soot formation in flames has been outlined in another review article by Frenklach [37].

According to Glassman [38], in *premixed* flames original fuel structures break down to acetylene and soot is formed in the high-temperature postflame zone. Such a mechanism may comprise elementary reactions involving a sequence of H-atom abstraction and acetylene addition reactions (HACA mechanism) [37] and formation of intermediates, such as vinyl, butadienyl, vinylacetylene, and phenylacetylene radicals. In recent years, in addition to the HACA mechanism, the importance of resonantly stabilized radicals in soot formation has also been established. These, relatively unreactive radicals, such as propargyl (C_3H_3 –), formed by the combination of vinyl and methyl radicals with subsequent hydrogen abstraction, may be building blocks of aromatic rings, particularly in the combustion of aliphatic fuels [39, 40]. In the case of aromatic fuels, such as benzene and the ethylbenzene of this study, the aromatic benzene ring is already present in the oxidation zone

and is mainly oxidized to cyclopentadienyl radicals ($c-C_5H_5$ –) [41]. As a consequence, a large amount of cyclopentadienyl radicals is immediately available for recombination reactions, leading to multi-ring aromatic formation. According to D’Anna and Violi [41], cyclopentadienyl self-combination is the dominant route in the multi-ring aromatic formation process in aromatic fuel flames. McEnally et al. [36] reported two more important reactions that form two-ring aromatic hydrocarbons, acetylene addition to 2-ethynylphenyl and propargyl addition to benzyl radicals. As the building blocks for large aromatic species formation are the main products of benzene oxidation, PAH are formed in the main oxidation zone of the flame [40,41]. The larger PAH compounds coagulate to form the first soot nuclei (soot inception), which are a few nanometers in size. These particles are initially transparent to visible radiation and exhibit spectroscopic properties typical of PAH with few condensed aromatic rings. These compounds are formed at a high rate in fuel-rich flames just downstream of the flame front and their concentration accounts for the total amount of soot formed under slightly sooting conditions. These nuclei continue to grow via surface reactions with acetylene, PAH, and other hydrocarbons present in the flame. Coagulation of growing soot particles leads to a decreasing number density while in total, particle mass remains constant [42].

Several studies have aimed to identify a quantitative specification of a fuel characteristic, such as the threshold soot index (TSI) [9,43,44], which is intended to help compare and analyze flame sooting data obtained in different experimental apparatus. The difficulty of setting up such a quantitative measure lies in that the local conditions, especially the temperature of the flame, drastically affect the soot onset limit even in the same experimental setup [9].

Flame temperature is very important in soot formation. Millikan expressed in his classic work [45] that the critical equivalence ratio (ϕ_c), where the incipient soot is visually first detected as a faint orange glow in the flame while the fuel/air mass ratio is increased from fuel-lean conditions, varies with the gas flow rate through the same burner even with all other parameters kept constant. Kaskan [46] showed that for a given equivalence ratio, the flame temperature can be changed by varying the cold gas velocity through the burner. Millikan concluded that increasing the (burned gas) temperature of a given *premixed* flame extends the soot threshold to higher equivalence ratios [45]. Surprisingly, though, readily sooting fuels (i.e., fuels with larger TSI) have been reported to have higher *calculated* flame temperatures at their critical equivalence ratios [47] compared to fuels which have relatively lower sooting tendencies.

Olson and Madronich [48] contrasted the effects of *calculated* and *measured* temperatures on soot threshold in premixed flames of toluene/O₂/N₂ and decalin/O₂/N₂ flames. They concluded that the soot yield for each fuel at and above the soot threshold limit is uniquely determined by the *measured* flame temperature in the sooting region (their measurements were at 20 mm from the surface of the burner, i.e., presumably in the burned gas), regardless of how this temperature was achieved. They pointed out that the narrow variation in *measured* temperatures at different ϕ_c was in marked contrast with the large variation of *calculated* adiabatic flame temperatures, over the same equivalence ratios they encountered. The *calculated* temperatures varied by about 280 K for toluene but the *measured* temperatures varied by only 12 K for the same range of equivalence ratios; they used an emission pyrometer for their temperature measurements. Böhm et al. [49] reported that the threshold of soot formation in flat flames depends on temperature, which they determined at 10 mm from the surface of the burner, using Kurlbaum's method [50]. With increasing temperatures, the critical C/O ratio, hence ϕ_c , increases. In contrast to Olson and Madronich [48], who reported that flames at different critical equivalence ratios experience the same *measured* temperature in the sooting region, Millikan [45], Böhm et al. [49], and Harris et al. [51] observed that the *measured* flame temperature increases in parallel to the critical equivalence ratio, ϕ_c . Moreover, the latter researchers reported that the observed linear relationship between $\ln(\phi_c)$ and $1/T$ also depends on the fuel, for five aliphatic fuels examined therein. "Obviously," Olson and Pickens [9] remarked, "flame temperatures are very important in soot formation and this relationship needs to be clarified." The work presented herein addresses the effects of the equivalence ratio on the soot onset limit, whereas future work will address the temperature effects.

Regarding the soot formation mechanisms, it has been reported that in premixed flames higher temperatures favor oxidation of light pre-aromatic-ring species over formation of soot precursors [34] and, thus, suppress soot formation [38]. (Whereas this work examines premixed flames, it is important to note that Sunderland et al. [35] have reported that the role of temperature is different in premixed and nonpremixed flames. Increased temperatures suppress soot formation in premixed flames, whereas they promote soot formation in nonpremixed flames. Initial detection of soot in diffusion flames has been observed at 1350 K (± 35 K) [53].) Markatou et al. [34] also suggested that the dependence of the critical equivalence ratio on temperature may be partly explained on the reversibility (as the temperature rises) of reaction steps leading to the formation and growth

of PAH. They concluded that factors that limit the production of PAH and, hence control the appearance of sooting limits, are the abundance of acetylene and the thermal decomposition/growth of PAH. This is consistent with the importance of the reverse reaction of ring closure via acetylene addition to naphthylacetylene radicals for the decreasing mole fraction of phenanthrene in a nearly sooting benzene flame [52].

Thus, the present work aims at decoupling the effect of temperature from that of equivalence ratio in the vicinity of the soot onset threshold. Its goal is to explore the effects of PAH chemistry on the soot onset, both experimentally, employing direct sampling in the flame and postflame region, and theoretically, using a chemical kinetic model. One-dimensional (flat) premixed flames were used, based on their uniformity with respect to flow-field, radial temperature profile, and particle size distributions.

The cold gas velocity through the flat flame burner was kept nearly constant. By adjusting the oxygen, the nitrogen, and the fuel flow rates, the maximum flame temperature was also kept nearly constant while the equivalence ratio was varied; hence, the observed change in PAH, and light hydrocarbon concentrations, if any, were related directly to fuel/oxygen ratio, independently of the effect of temperature. The mole fractions of characteristic soot precursors along with fixed gases were compared at the critical equivalence ratio, where soot was first visible in the flame, and slightly beyond. Flames in the vicinity of the soot onset threshold were chosen in an attempt to better isolate the chemical reactions that are responsible for soot inception from physical phenomena such as condensation, coagulation, agglomeration, etc. The concentrations of some oxygenated compounds were also measured to monitor the effect of fuel/oxygen ratio on oxidation reactions of aromatic hydrocarbons, again, isolated from the effects of temperature. The experimental results were then contrasted to the predictions of a detailed chemical model, previously tested with considerable success in conjunction to premixed, sooting benzene and ethylbenzene flames [28,54]. Information gathered was used for assessing the adequacy of reaction pathways involved in soot formation as currently implemented in the model.

2. Experimental apparatus and procedure

Atmospheric pressure, premixed, laminar flat-flames were stabilized on a 50.8-mm-diameter sintered bronze burner Fig. 1. The burner temperature was controlled with air flowing through embedded copper tubing. Flames were isolated from the ambient air by a concentric sheath flow of N₂, at a velocity of 5.3 cm s⁻¹, at STP. Flames were stabilized with a per-

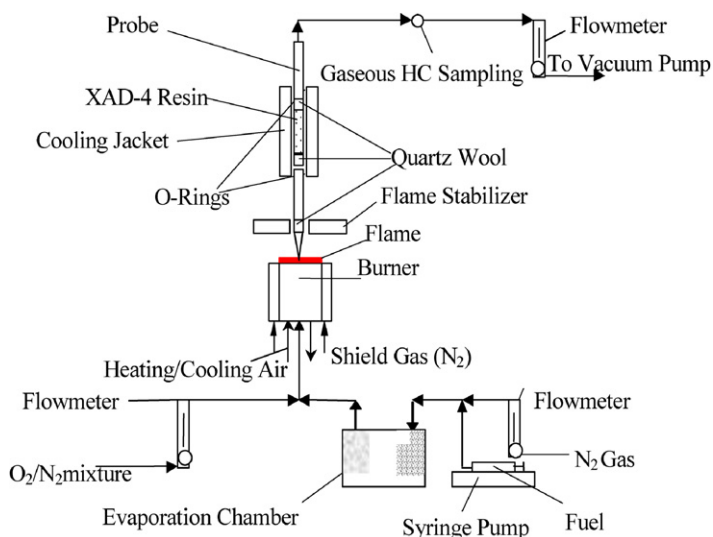


Fig. 1. Burner and sampling setup.

forated plate, positioned 30 mm from the burner surface and water-cooled with a copper coil. Liquid ethylbenzene (from Fisher Scientific/ Aldrich), placed in 50-ml glass syringes (Hamilton) and driven by a dual infusion/withdrawal syringe pump (World Precision Instruments Inc.), was introduced to a stainless-steel vaporizer (2 L in volume) equipped with a nitrogen-flow-assisted atomizer. The vaporized fuel–nitrogen mixture was introduced to the bottom of the burner, through heated tubing, and it was mixed with a preheated oxidizing gas mixture (50 vol% O₂–50 vol% N₂). The vaporizer and the tubing were heated to a temperature 20–50 °C higher than the boiling point of ethylbenzene, which is 137 °C. The ensuing mixtures were composed of the following mole fractions: (a) for $\phi = 1.68$: 0.269 oxygen, 0.688 nitrogen, 0.043 fuel; (b) for $\phi = 1.74$: 0.284 oxygen, 0.669 nitrogen, 0.047 fuel; (c) for $\phi = 1.83$: 0.264 oxygen, 0.690 nitrogen, 0.046 fuel. As experiments were repeated in triplicate to measure both temperatures and species concentrations, a sensitivity analysis was conducted. Based on readings from flowmeters (precalibrated rotameters and mass flowmeters), the equivalence ratios during each of the tests were within ± 0.05 of the aforementioned average values. The initial cold gas velocity for all of the flames was $7.79 \pm 0.12 \text{ cm s}^{-1}$ (at 1 atm, 25 °C) (see Section 4). Product gases were withdrawn from different heights in the flames by a quartz probe, cooled with water flowing through a copper cooling jacket around the probe [55]. A 1-cm i.d. quartz probe was used, with a tip diameter of 4.4 mm. The quartz probe was kept in the flame before sampling started for a duration that was sufficiently long to allow its tip to equilibrate with the flame temperature, in order to minimize disturbance of the temperature field in the flame. Sampling was

performed isoaxially and isokinetically to minimize the disturbance of the flow field. Flow rates corresponding to isokinetic conditions were determined based on an experimentally derived temperature profile.

2.1. Sampling procedure

Sampling measurements were conducted at 1, 3, 5, 7, and 9 mm above the burner; hence they took place both inside the flame and in the postflame zone. The probe was cut into two sections at a distance of 75 mm from the tip. The bottom portion, containing the tip, was sealed into the cooling jacket with two o-rings to prevent leaks and to keep the piece in a straight position. Quartz wool (from Ohio Valley Specialty Chemical) was positioned 10 mm above the tip, to capture condensed species. The advantage of this arrangement is that the quartz wool may easily be inserted into and removed from the probe without significant losses by deposition to the walls of the probe. The remaining 310-mm part of the probe was inserted into the cooling jacket from above through another o-ring, which prevented leaks. In this part of the probe, precleaned XAD-4 resin adsorbed volatile PAH not captured by the glass wool.

2.2. Sample analysis

Upon termination of each experiment, quartz wool and XAD-4 were removed and placed in precleaned vials. Methylene chloride was used to wash the interior of the probe and then it was also collected to account for the loss of PAH condensing on the inner walls of the probe. The samples were then spiked with deuterated standards of naphthalene-*d*8,

acenaphthene-*d10*, anthracene-*d10*, chrysene-*d12*, and perylene-*d12*. After extraction with methylene chloride in a Dionex ASE 200 accelerated solvent extractor, analysis was conducted by gas chromatography coupled to mass spectrometry (GC–MS) using a Hewlett–Packard (HP) Model 6890 GC with an HP Model 5973 mass selective detector. Details of analysis and calibration have been reported previously [23,24,28]. Samples of light gaseous hydrocarbons and fixed gases were collected with gas-tight 1-ml glass syringes downstream of the probe (see Fig. 1), and were injected into an HP 6890 Series GC with flame ionization and thermal conductivity detectors (GC-FID/TCD). O₂, CO, CO₂, C₁–C₄, and single-ring aromatic hydrocarbons were quantified with two parallel columns (100/120 Carbosieve S-II and HP-5/Al₂O₃ capillary column). The instrument was calibrated regularly with CO–CO₂ mixtures and with Scotty IV analyzed gas mixtures containing known concentrations of C₁ to C₄ aliphatic hydrocarbons and single-ring aromatics.

2.3. Temperature measurements

Temperature measurements were conducted along the centerline of the flame with four Pt/Pt–10%Rh (type-S) Omega thermocouples, with bead diameters of 0.076, 0.178, 0.356, and 0.762 mm. The measurements were conducted individually for each thermocouple in order to minimize disturbances in the flame. Each measurement was repeated at least three times, in some cases up to seven times, in order to monitor the repeatability of the temperature measurements. In most cases, the repeatability was good with standard deviations being within 30 K, especially in the postcombustion region, at 1.5 mm from the surface of the burner and higher. There were steep temperature gradients between the surface of the burner and the flame front. Therefore, the measurements in this region (the first 1–1.5 mm above the surface of the burner) proved to be very sensitive to the location of the thermocouple. The vertical spatial resolution of the thermocouple-positioning device was ± 0.1 mm. Especially for the thickest thermocouple ($d_{\text{bead}} = 0.762$ mm), the size of which is comparable to the length of the steep temperature gradient region, the repeatability of measurements was not as good as with the thinner thermocouples. The standard deviations of these measurements were higher, reaching 200 K.

Upon completion of the temperature measurements, radiative heat losses from the thermocouple beads needed to be accounted for to determine the “true” flame temperature. The pertinent method used herein is a modified Nichol’s extrapolation method and it is briefly outlined below, whereas details are

given elsewhere [56]. In lieu of correcting for the ill-defined radiative heat losses [56,57], recorded temperatures were plotted as a function of bead size and, upon extrapolation to “zero” bead size, the intercept presumably corresponds to the true flame temperature [58]. Regarding the nature of the extrapolation the following observation was made; when a third-order polynomial curve was fitted to the temperatures measured with four thermocouples, the extrapolation resulted closer to the true flame temperature than a straight-line extrapolation [56]. This was tested theoretically and also experimentally by comparing the results obtained by extrapolation to the ones obtained with theoretical heat loss corrections as discussed below. Hence, four different-sized thermocouples were used, as this is the minimum number of data points to fit a third order polynomial. The intercept of the third-order polynomial fit with the ordinate (i.e., at zero bead size) was recorded as the flame temperature. Corrections for soot accumulation on the thermocouple beads were not necessary, since no soot was present visually on the thermocouples for neither of these nearly sooting flames.

The temperatures obtained with this extrapolation method are presented in Fig. 2. The three flames around the sooting limit ($\phi = 1.68, 1.74, 1.83$) have similar temperature profiles, the maximum temperatures of which are 1878 ± 10 K. The temperature profile of the highly sooting flame ($\phi = 2.5$) of the previous study [28] is also included for comparison. The maximum temperature of the latter flame is approximately 200 K cooler than the three flames in the vicinity of the soot onset limit. Moreover, after the flame (maximum temperature) region, the highly sooting flame cools down faster. In the postflame region the temperature difference between the highly sooting flame and the flames in the vicinity of the sooting limit increases up to ~ 420 K at 15 mm from the surface of the burner. Enhanced radiative losses in the heavily sooting flame ($\phi = 2.5$) most likely contribute to its accelerated cooling.

To test the reliability of the method, a theoretical correction for radiative losses was also performed using a quasi-steady energy balance at the junction, as suggested by McEnally et al. [59],

$$\frac{\text{Nu}_b k_{g0}}{2d_b} (T_g^2 - T_b^2) = \varepsilon_b \sigma T_b^4, \quad (1)$$

where ε_b is the emissivity of the thermocouple bead, σ is the Stefan–Boltzmann constant, d_b is the diameter of the bead, and T_b is the temperature recorded by the thermocouple bead. $k_{g0} \equiv k_g/T_g$, where k_g is the gas thermal conductivity and T_g is the gas temperature. k_{g0} was taken as a constant, assuming k_g depends linearly on gas temperature, which is suggested to be a reasonable assumption for combustion

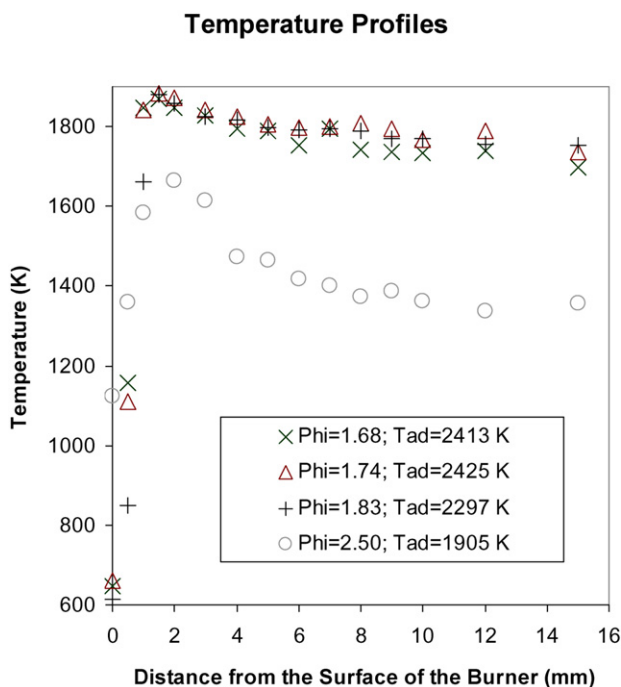


Fig. 2. Temperature profiles of nearly or slightly sooting flames ($\phi = 1.68, 1.74, 1.83$) together with the temperature profile of a highly sooting flame ($\phi = 2.5$) [28]. Equilibrium adiabatic flame temperatures were calculated using the STANJAN code [60].

gases at high temperatures [59]. Nu_b is the Nusselt number for the thermocouple bead.

When this correction was applied to the measurements of each thermocouple, considerable discrepancies were found in the temperatures obtained from different size thermocouples at a specified location in a given flame. Flame temperatures were higher from the measurements obtained with the thicker thermocouples than from those with the thinner thermocouples. Since the spatial resolution in the flame with the thinner thermocouples is better, and since they disturb the flame less, the measurements with the thinnest thermocouple ($d_b = 0.076$ mm) were assumed to be the most dependable flame temperature measurements, upon making theoretical corrections. In fact, the corrected measurements of the thinnest thermocouple were within 50 K of the temperatures obtained with the aforementioned modified Nichol's extrapolation method, where extrapolation was done with a third order polynomial.

Equilibrium adiabatic flame temperatures were calculated using the STANJAN code [60] and are also listed in Fig. 2. To attain the listed values, input to the code were the pertinent mole fractions of the fuel, oxygen, and diluent used in these experiments, as well as the measured preheated gas temperatures at the burner. As expected, the calculated temperatures were higher than the measured values because calcu-

lations did not account for heat losses from the flame to the burner and the surroundings.

3. Experimental results and discussion

3.1. Visual investigation

In order to visually assess the sooting limit, flat flames were stabilized over the burner. Initially, the strongly fuel-rich ($\phi = 2.5$) flame of previous work [28] was gradually made leaner by decreasing the fuel flow rate. As the burning velocity changed with varying equivalence ratio, to stabilize the flame the flow rate of the carrier gas (nitrogen) was adjusted to ensure steady and effective fuel atomization and vaporization. Consequently, the flow rate of oxygen was also changed and it was thereby observed that the soot onset limit in premixed flames is a complex function of mixture composition, temperature and flow characteristics of the reacting gases. Temperature is a function of equivalence ratio among other parameters, such as cold gas velocity, initial temperature of the gases, type of the diluent, and oxygen/diluent ratio. Hence, it is not feasible to identify a unique critical equivalence ratio (ϕ_c) for a given fuel, where the equivalence ratio is defined as $\phi = [(m_{\text{fuel}}/m_{\text{oxygen}})_{\text{actual}}]/[(m_{\text{fuel}}/m_{\text{oxygen}})_{\text{stoichiometric}}]$. Depending on the temperature, the soot inception may commence at any ϕ , in

a certain interval, which is determined by the stability of the flame over the burner surface of a particular setup. In this study, the visual onset of soot was observed at equivalence ratios between $\phi = 1.68$ – 1.88 for ethylbenzene/O₂/N₂ flames, by varying the total gas flow rate and the O₂/N₂ ratio through the burner. The flames in this work were selected for investigation because not only similar maximum *measured* temperatures were attained, but also similar spatial temperature profiles throughout the important initial in-flame region as well as throughout the ensuing postflame region were obtained; see Fig. 2.

It was also observed that as the flow rate of the fuel was reduced, keeping the flow rates of O₂ and N₂ constant, the intensely luminous nearly white/orange zone downstream of the flame sheet elongated. Hence, as the equivalence ratio decreased from $\phi = 2.5$ to $\phi = 1.9$, the luminous postcombustion zone for the flame extended upward till it reached the flame stabilizer plate; see Fig. 3. The shortening of the luminous flame at high equivalence ratios may be attributed to the increased heat losses because of rising particulate loading and, thus, radiating particulate surface area. Since more soot is generated in the postflame zone, more heat is lost prior to reaching the stabilization plate. As soot particles cool down they lose their luminosity. In relatively leaner flames, the total soot surface area is less extensive, thereby reducing the collective heat loss and preserving luminosity. At even leaner mixtures the flame lost its luminosity, as the soot particle loading drastically decreased and the yellow color faded. Finally, at a certain ϕ /temperature combination, soot completely disappeared. As the equivalence ratio decreased, in the fuel-rich domain, the temperature of the flame increased. To keep the flame temperature constant in a narrow range of equivalence ratios around the soot onset limit, both the oxygen and the nitrogen flowrates were varied. This adjustment procedure was complicated by the objective to also keep the total cold gas velocity through the burner constant for the targeted flames, shown in Fig. 4. Although the maximum recorded temperatures of these flames were similar (see Fig. 2), the flames themselves were not visually equivalent.

3.2. Concentrations of combustion species

Mole fractions of major light hydrocarbons, along with O₂, CO, and CO₂, are shown in Fig. 5 and PAH species are shown in Fig. 6. The mole fractions of corresponding species found in the highly sooting ethylbenzene flame ($\phi = 2.5$) of the previous study [28] are also discussed for comparison. The reader may note however, that the temperature profile of this highly sooting flame is considerably lower when compared

to the temperature profiles of the three nearly sooting flames (see Fig. 2). One may also note that there was more diluent (65–72 mol% N₂) in the product gases of the nearly sooting flames as compared to highly sooting flame (54–58 mol% N₂), based on the total amount of gas in the product. Hence, the higher mole fractions of the products observed in the highly sooting flame are partly due to the lower amount of nitrogen in this case. Because of these reasons the absolute values of species concentrations from the highly sooting flame should not be directly compared to those from nearly sooting flames. In the following, the flames are labeled according to their equivalence ratios as Flame_{1.68}, Flame_{1.74}, Flame_{1.83}, and Flame_{2.5}. The list of mole fractions of the species discussed in the text, and plotted in Figs. 5, 6, 7, and 8, can be found in tables in Appendix A.

The first difference between the Flame_{1.68} and the other two slightly sooting flames is that O₂ is consumed in the postflame region in the former case (the leanest flame), while the oxygen concentrations in the slightly sooting flames were nearly constant. In all cases, O₂ was consumed to less than 1 mol% within the first 1 mm from the surface of the burner (Fig. 5). The CO mole fractions increased with distance from the burner in each flame; for Flame_{1.68} from 12.8 to 17.4%, for Flame_{1.74} from 14.3 to 17.4% and for Flame_{1.83} from 13.1 to 17.3%; see, Fig. 5. In contrast, the CO mole fraction in the highly sooting Flame_{2.5} increased from 20 to 24% [28]; see also Fig. 8 in a subsequent section of this manuscript. Conversely, the CO₂ mole fractions exhibited decreasing trends along the axes of the flames. In Flame_{1.68} and in Flame_{1.74} the CO₂ mole fraction dropped from around 9 to 7.5%, whereas in Flame_{1.83} it dropped from 9 to 6.3%. In the highly sooting Flame_{2.5} the CO₂ drop was from 4.8 to 4.2%, although an initially increasing trend was observed in the first 7 mm from the burner surface; see Fig. 8.

The profiles of the major detected light aliphatic hydrocarbons (methane, ethane, ethylene, acetylene) exhibited in some cases a slight increase in the postflame region, followed by precipitous decreases thereafter. This behavior contrasts with that observed in the highly sooting flame, where mole fractions of two of these species (methane and acetylene) increased along the flame axis, while the other two either remained constant or mildly decreased; see Fig. 8. It is interesting to note that acetylene, which has been linked to PAH and soot generation, was found to be present in similar amounts in all flames (see the first sampling point). Thereafter, it was consumed inversely proportional to ϕ . Furthermore, it remained elevated in the highly sooting flame ($\phi = 2.5$), paralleling the experimentally determined soot concentrations therein; see Fig. 8. To the contrary, in the case of

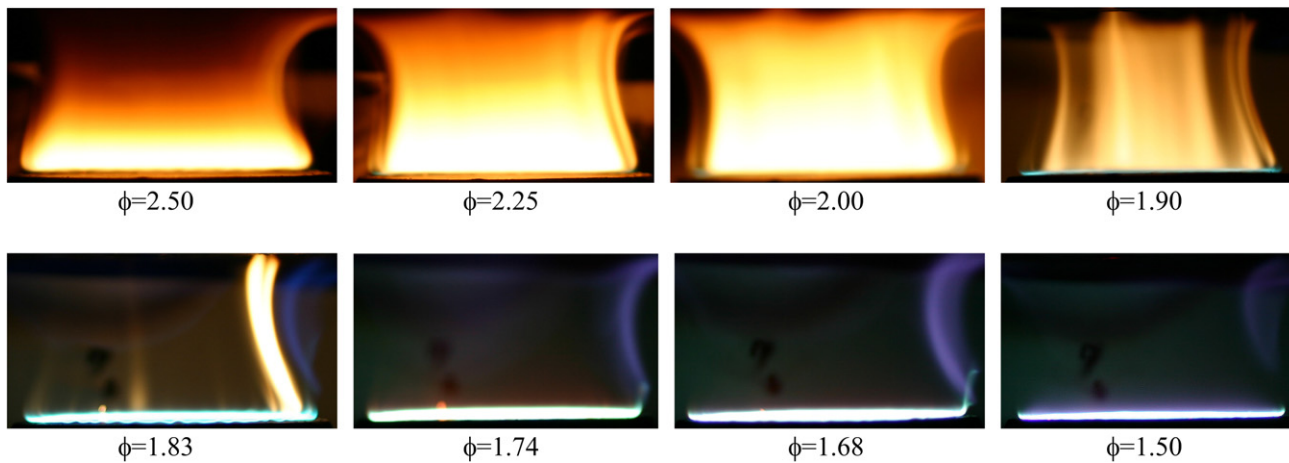


Fig. 3. Visual investigation of soot onset limit in ethylbenzene flames with respect to equivalence ratio.

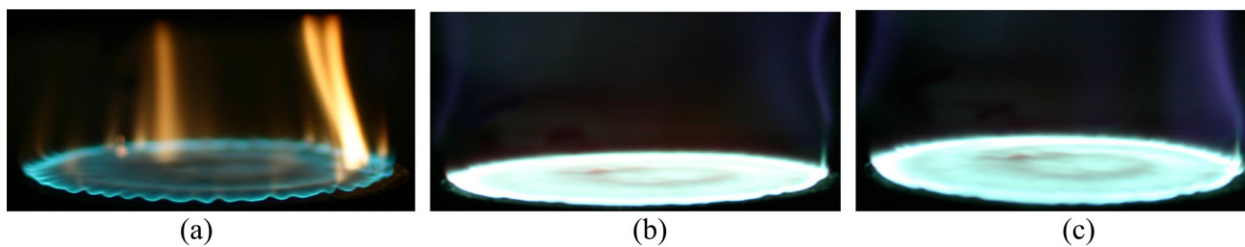


Fig. 4. Ethylbenzene flames with similar measured maximum temperatures: (a) $\phi = 1.83$, (b) $\phi = 1.74$, (c) $\phi = 1.68$.

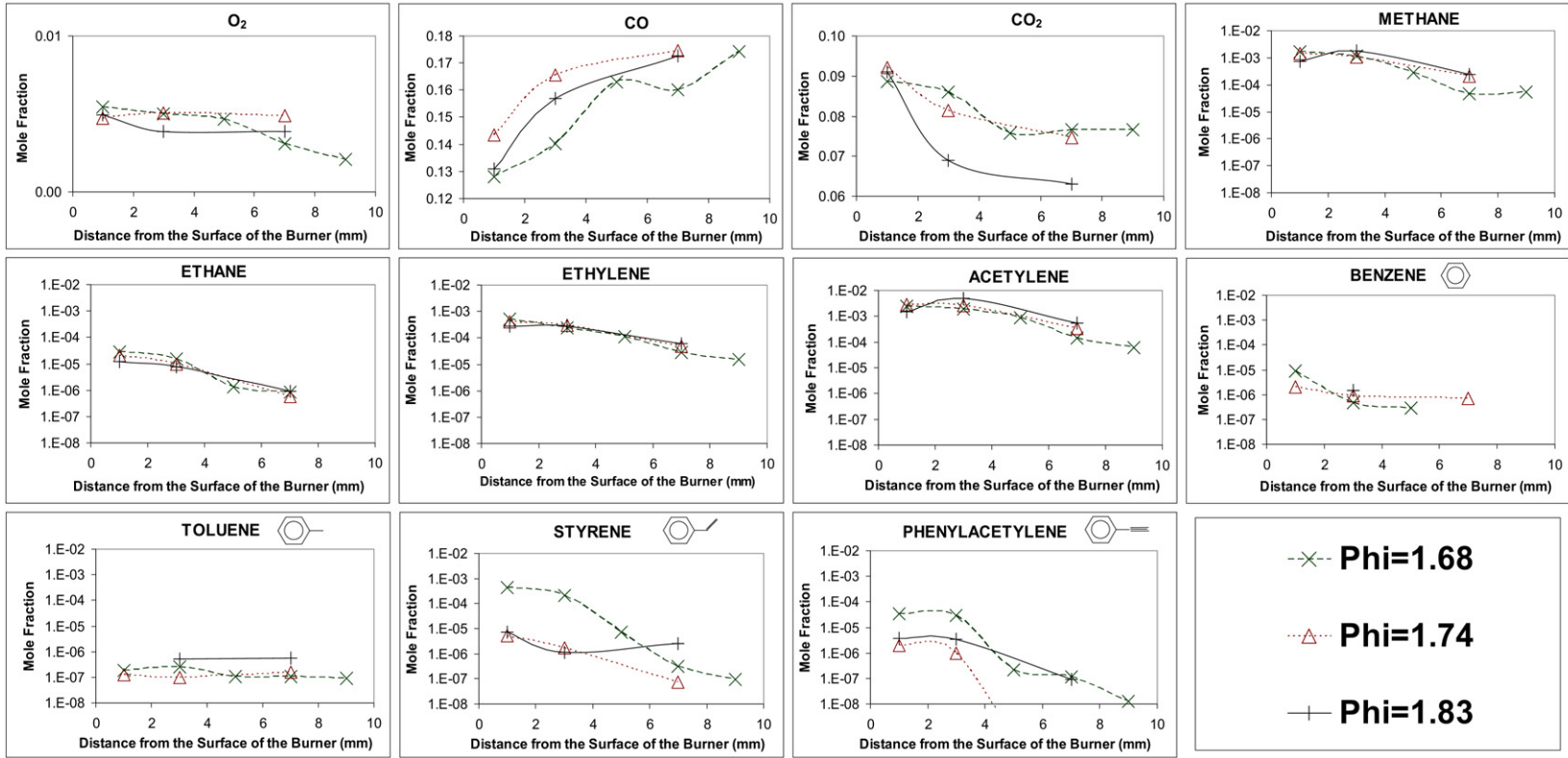


Fig. 5. Fixed gases and light hydrocarbons in nearly sooting and slightly sooting flames ($\phi = 1.68, 1.74, 1.83$). Logarithmic scale is used for hydrocarbons only. For the exact experimental values see Appendix A.

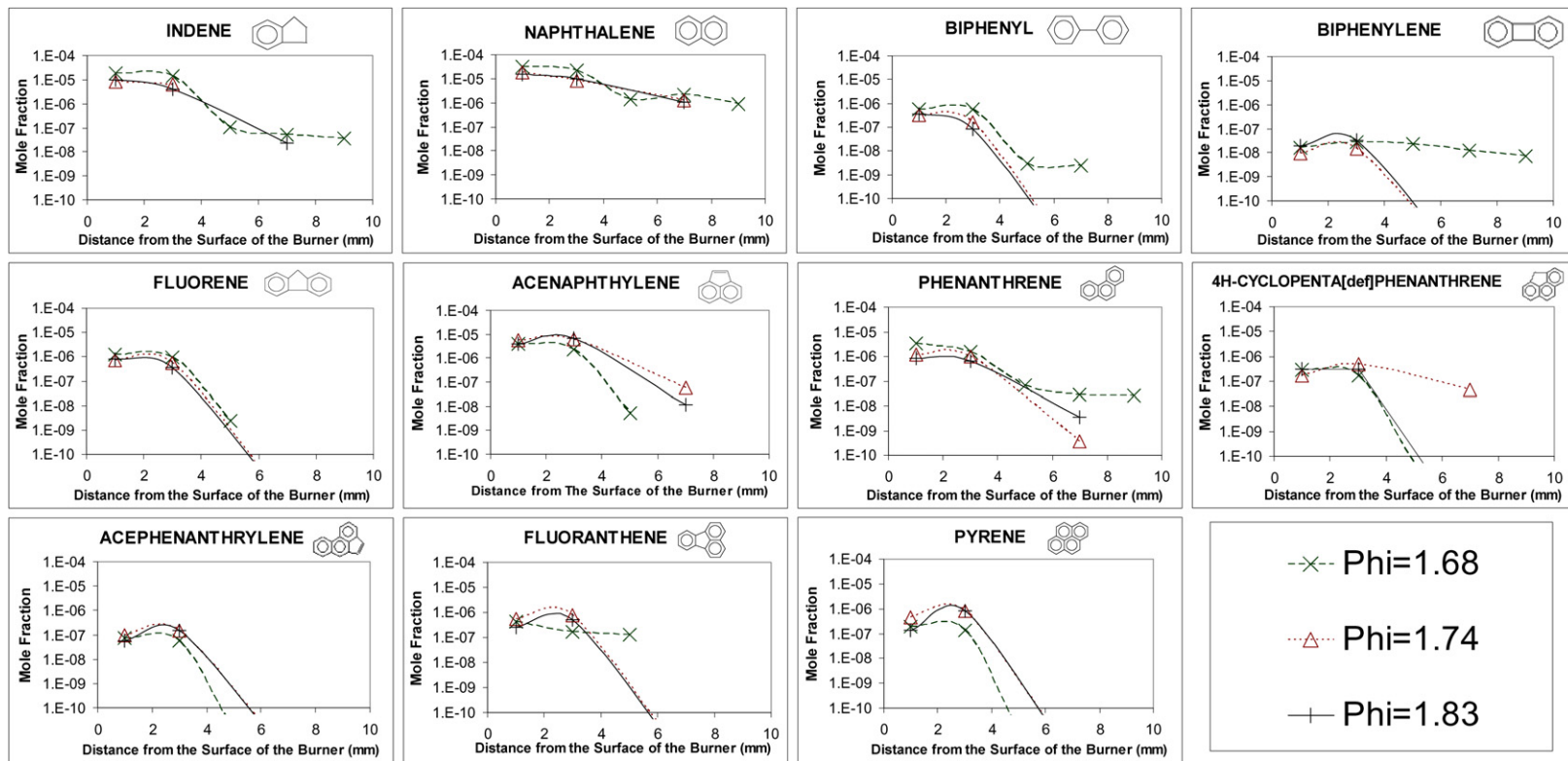


Fig. 6. PAH concentrations in nearly sooting and slightly sooting flames ($\phi = 1.68, 1.74, 1.83$). For the exact experimental values see Appendix A.

the three nearly sooting flames the decreasing acetylene profiles parallel the decreasing profiles of PAH and are in line with the absence of detected soot, especially in the case of Flame_{1.68}. The initial mole fractions of styrene and phenylacetylene were much higher in Flame_{1.68} than in Flame_{1.74} and Flame_{1.83}. As styrene is an important component of the ethylbenzene pyrolysis scheme, this may be an indication that the appearance of soot in the latter flames consumed styrene at constant temperature. Mole fractions of benzene and toluene were of the same order of initial magnitude in all flames. In the postflame region phenylacetylene and styrene were consumed, whereas the benzene and toluene mole fractions varied by only a little along the flame/postflame region. Although all of these compounds (benzene, toluene, styrene, and phenylacetylene) contain a benzene ring, they all differ with respect to the functional group on the ring, and the reactivity of the functional group with soot. Benzene has no functional group and hence no functional group reactivity. Toluene has a methyl group which, like methane, is relatively (compared to other hydrocarbons) unreactive with soot. The groups on styrene and phenylacetylene, i.e., ethylene and acetylene, have relatively high reactivities with soot. These soot-reactivity differences are so large as to give, under the present conditions, a consumption by soot that is almost nil for benzene and toluene but considerable for styrene and phenylacetylene. Continued formation or oxidation may also be responsible for such differences between concentration profiles in the postflame zone. It should be kept in mind that concentration profiles are the result of a tight balance between formation and consumption of a given species and that relatively small changes in rates of specific reactions can have a significant impact.

Mole fractions of major polycyclic aromatic hydrocarbons (PAH) are shown in Fig. 6. The trends along the three flames in the vicinity of the soot onset experience parabolic or continuously decreasing profiles. Mole fractions at the exit of the post combustion zone are often very low, even below the detection limit of the GC/MS system. The demise of PAH in the upper postcombustion zone may be aided by the elevated temperatures found in these nearly sooting flames, throughout their postcombustion regions (see Fig. 2), leading to enhanced oxidation and possibly reverse reactions. In contrast, Flame_{2.5} was far richer and less hot than the three aforementioned flames on the verge of sooting; i.e., its conditions favored the formation and survival of PAH [20]. Hence, along the axis of that flame, PAH mole fractions did not decrease much [28]; see Fig. 8.

The relative abundance of PAH species in the three nearly sooting flames, which had almost the same flame temperatures, was comparable (see first

data points in the plots of Fig. 6). Thereafter, in the postflame zones, the low-molecular-weight PAH were more abundant in the case of the nonsooting Flame_{1.68}, whereas the high-molecular-weight PAH were more abundant in the other two flames. Furthermore, in the postflame zones of the two slightly sooting flames (Flame_{1.74} and Flame_{1.83}) there was occasionally an initial mild increase in mole fraction with axial distance, probably leading to initial soot formation. This was followed by precipitous consumption by oxidation or, more likely, consumption by surface growth of soot particles. Profiles of many low-molecular-weight PAH species in the nonsooting Flame_{1.68} exhibited less steep, rather continuously decreasing trends. In contrast, mole fractions of most of the higher-molecular-weight PAH (4–5 ring aromatics) and acenaphthylene decreased faster in this flame. As scavenge of PAH into soot was not observed in the case of nonsooting Flame_{1.68}, the most likely consumption pathways therein involve oxidation reactions and reverse reactions of ring closure via acetylene addition [52].

Plots of detected oxygenated PAH are included in Fig. 7, the most pronounced being benzaldehyde and phenol. Other detected oxygenated PAH include benzofuran, 2-naphthalenecarboxaldehyde, dibenzofuran, fluorene-9-one, and 9,10-anthracenedione. Lending support to the importance of PAH oxidation, it is evident that the nonsooting Flame_{1.68} contains higher mole fractions of these compounds than the slightly sooting Flame_{1.74} and Flame_{1.83}.

The total PAH mole fractions in the postflame region (as measured at 7 mm height above the burner) decreased by an order of magnitude as the equivalence ratio increased from nonsooting conditions ($\phi = 1.68$) to the soot onset limit ($\phi = 1.74$). Thereafter, the total mole fraction of PAH dropped mildly until $\phi = 1.83$ was reached (values are shown in Appendix A). This behavior will be further investigated in future work.

4. Experimental error analysis

The data reported above is the average of three measurements at each location in every flame. The uncertainties in these measurements may be classified in three categories: (i) Uncertainties in the flame composition due to limitations in the precision of measuring devices. (ii) Uncertainties in the sampling process, as during sampling and transfer of samples, some—especially the most volatile PAH—may be lost. (iii) Uncertainties of extraction and quantification, since although the extraction efficiencies are satisfactory, there are some uncertainties during GC/MS analysis too. In the following, these uncertainties are discussed.

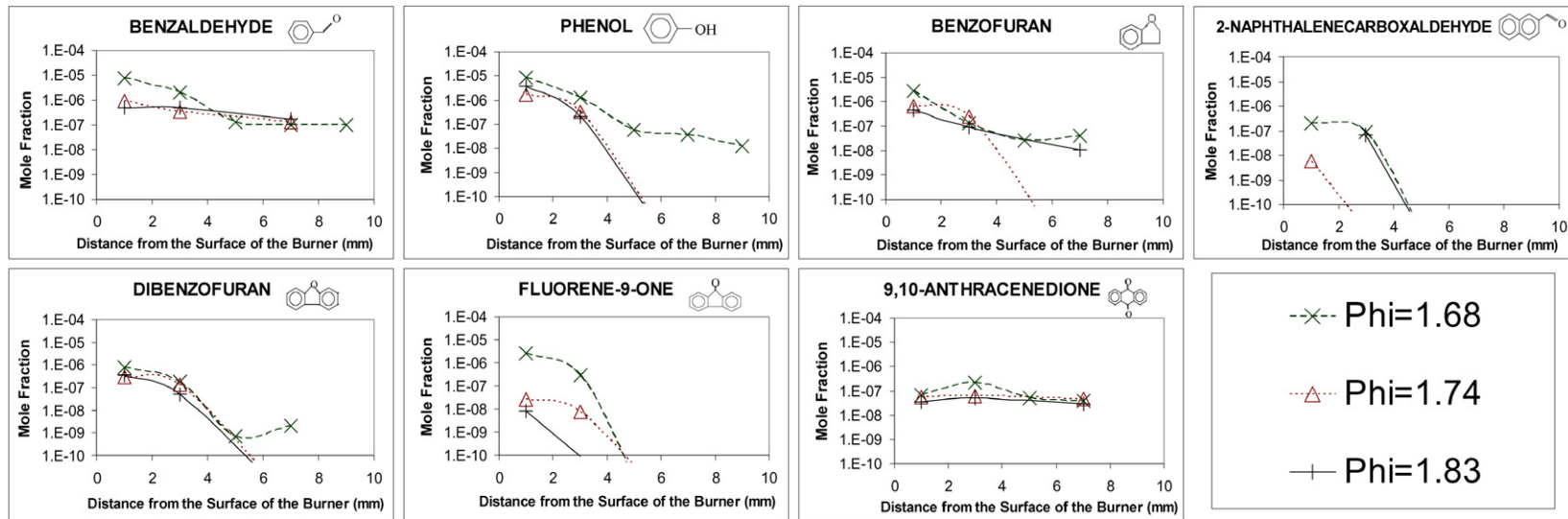


Fig. 7. Mole fractions of oxygenated compounds in nearly sooting and slightly sooting flames ($\phi = 1.68, 1.74, 1.83$). For the exact experimental values see Appendix A.

The syringe pump that was used to inject the fuel into the vaporization chamber is reported to have an accuracy of $\pm 1\%$ of intended flow rate. The high-precision flow meters used have an uncertainty of ± 0.1 lpm for O_2/N_2 mixture and ± 0.04 lpm for dilution nitrogen. The accumulated error caused by these uncertainties may affect the calculated equivalence ratios within ± 0.05 . Hence, although tests were performed controllably, the three nearly/slightly sooting flames may in extreme cases be between $\phi = 1.63$ – 1.73 (Flame_{1.68}), $\phi = 1.69$ – 1.79 (Flame_{1.74}), $\phi = 1.78$ – 1.88 (Flame_{1.83}). Moreover, the cold gas velocity may be within ± 0.12 cm s⁻¹ of the value reported above ($V_{\text{coldgas}} = 7.79$ cm s⁻¹).

The extraction efficiencies were typically well above 80% for most PAH species, but dropped down to 60% for some volatile species, such as naphthalene, in some cases. Mean values and standard deviations are calculated from three repeats for each of the data points reported above. If two of the repeats were in good agreement, while the third repeat did not agree as well, this third repeat was not included in the averages reported above. Percent deviations (standard deviation/mean $\times 100\%$) are calculated for each point reported. The deviations of the points closer to the flame were larger compared to the deviations of samples taken at higher locations in the post flame region; this may be attributed to large temperature gradients existing around the flame front. Because of these large gradients, the vertical spatial resolution of the tip of the probe has a great effect on the sampled species. In all of the flames, percent deviations reached up to 160% for some species (usually for lower molecular weight species) in the lowest sampling location (1 mm from the surface of the burner). In other sampling locations the percent deviations were consistently lower, reaching as low as 1% for some species. These deviations are again, due to the accumulated effects of all three factors listed above.

5. Kinetic modeling

A kinetic model describing the formation and consumption of PAH and carbonaceous material (soot) has been developed and successfully tested [54]. Modeling calculations were conducted for all investigated conditions using experimental temperature profiles. Numerical predictions were compared to data and observations qualitatively assessed. Using a sectional approach [61], large PAH and carbonaceous particles with diameters of up to ≈ 70 nm are defined as classes (BINs) covering given mass ranges [54]. Recently, thermodynamic property data of PAH were updated using a consistent set of data derived from high-level quantum-chemical calculations [62] allow-

ing differentiation between all major isomers and radical sites. Model calculations for sooting [63] and nearly sooting [64] low-pressure flames showed significant additional improvements in the predictive capability of the model. All model computations were conducted with the Premix code of the CHEMKIN software package [65] using the experimental temperature profile. Different from earlier versions of this software, the unmodified gas phase Interpreter now allows the handling of molecules with numbers of carbon and hydrogen atoms sufficiently large to correspond to soot particles of increasing size. Pressure dependence of chemically activated reactions was addressed using quantum Rice–Ramsperger–Kassel analysis [66] and corresponding rate constants were determined for atmospheric pressure conditions. In the previous work, the model was refined for the first decomposition steps of ethylbenzene; pertinent reactions were taken from the literature or estimated [28]. Thermodynamic data of Burcat [67] were used for ethylbenzene, whereas data for $C_6H_5CHCH_3$ (C_8H_9) were obtained subsequently using group additivity [68] based on bond dissociation of a secondary benzyl group. The resulting reaction mechanism consisted of 335 species and 8086 reactions. Oxidation of intermediates of ethylbenzene depletion with O, OH, and O_2 is also included in the model. This model has been used previously for the description of fuel-rich ethyl alcohol flame and the above-mentioned highly sooting ethylbenzene flame [28]. The predictive capability of the model for PAH was found to be satisfactory in both cases. The ethyl alcohol flame did not generate significant amounts of soot, neither in the experiments nor in the model prediction, and the predicted soot concentrations for ethylbenzene agreed with gravimetrically determined data within the limits of the experimental uncertainty [28].

Results of the kinetic model are shown in Fig. 8, where experimentally detected mole fractions of selected combustion byproducts are compared with model predictions. This time, the results of the heavily sooting fuel-rich flame, examined in previous work [28], were also included to illustrate the predictions of the model at various conditions. The model predicted fairly well the CO and CO_2 mole fractions in the flames (including the postflame regions). It nearly reproduced the oxygen mole fractions throughout the heavily sooting Flame_{2.5}, but somewhat underpredicted the mole fractions in the postcombustion zones of the nearly sooting flames. It overpredicted the magnitude and the trend of acetylene mole fractions, and similarly overpredicted the corresponding soot emissions. Remarkably, the model's predictions of acetylene mole fractions throughout the heavily sooting flame were very good and, consistently, the corresponding soot predictions were also successful.

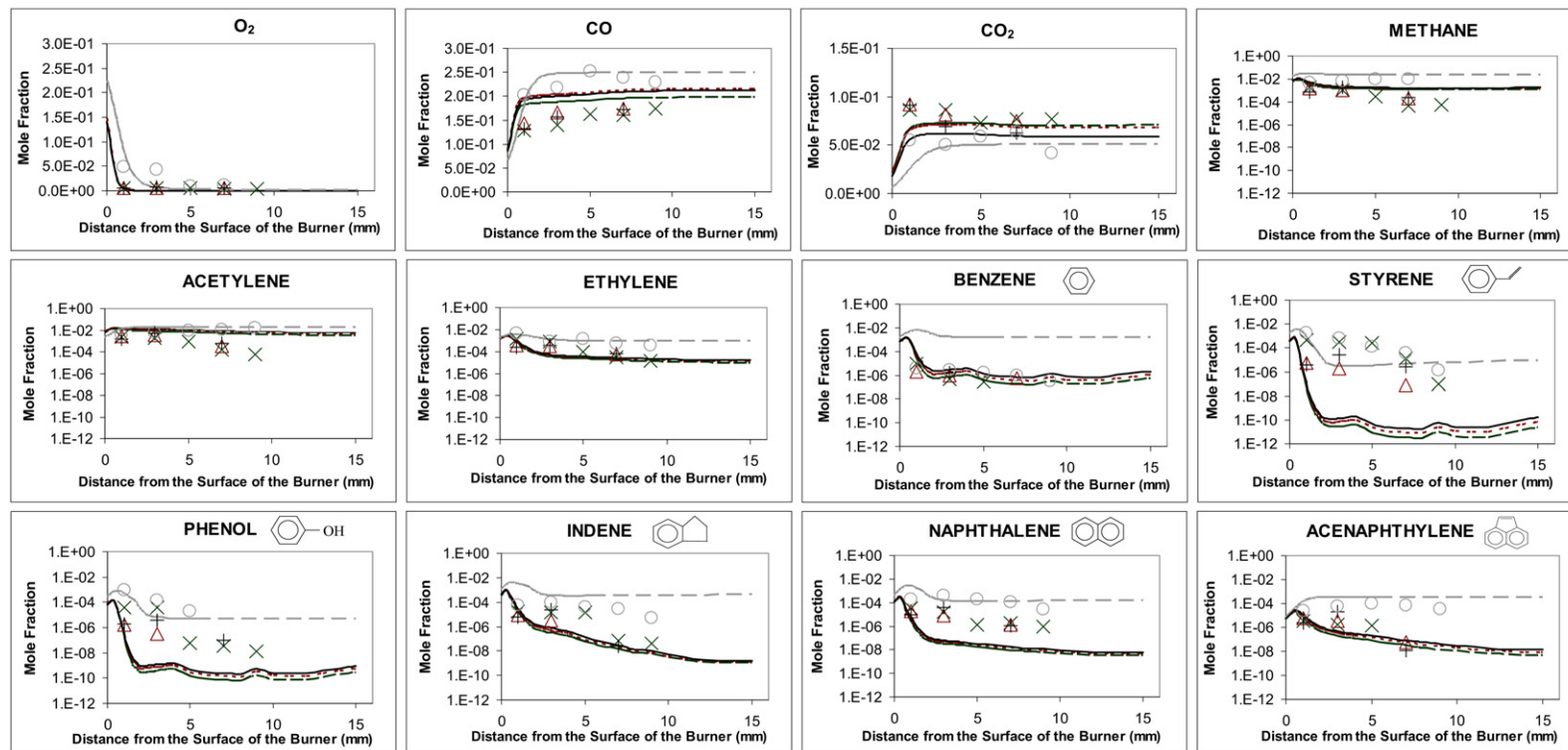


Fig. 8. Comparison of model predictions to the experimental data for nearly sooting and slightly sooting flames ($\phi = 1.68, 1.74, 1.83$) together with highly sooting flame ($\phi = 2.5$) from Ergut et al. [28]. Logarithmic scale is used for the hydrocarbons only. For the exact experimental values see Appendix A.

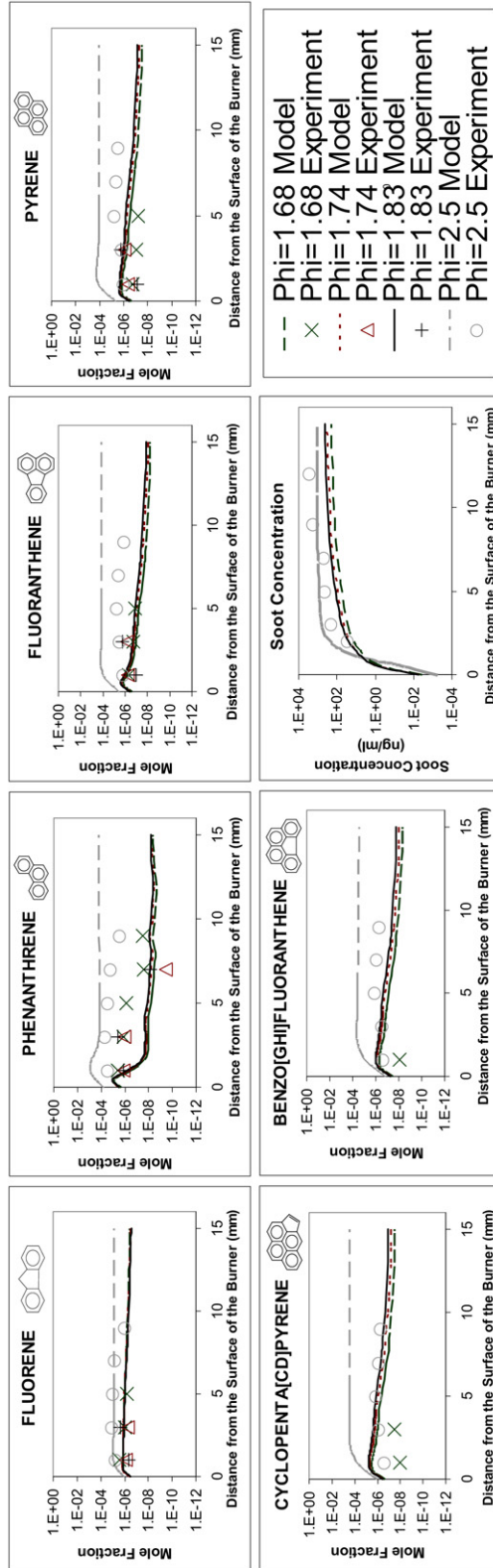


Fig. 8. (continued)

This clearly underlines the importance of acetylene in soot formation and it shows that in nonsooting or nearly sooting flames there are mechanisms that consume acetylene fast in the flame/postflame regions and prevent the formation of soot. This underscores the importance of incorporating detailed oxidation reaction mechanisms in the model which may be responsible for the fast consumption of acetylene. The model was rather successful in its predictions of ethylene and ethane (the latter not shown in Fig. 8) for all flames, and for benzene in the case of the three nearly sooting flames. However, it underpredicted toluene (not shown in Fig. 8), phenol, styrene, and naphthalene in the case of the nearly sooting flames, whereas it was more successful in its predictions in the case of the heavily sooting flame. It was more successful in the cases of 3 and 4-ring PAH, exhibiting outstanding fidelity in the case of fluorene and acenaphthylene for all flames; good fidelity for fluoranthene and pyrene in the cases of the nearly sooting flames. Naphthalene, which was fairly well predicted in the highly sooting flame, was underpredicted in the nearly sooting flames, and so was phenanthrene. For higher molecular weight species, the model overpredicted their mole fractions (e.g., cyclopenta[cd]pyrene and benzo[ghi]fluoranthene in Fig. 8).

The last plot in Fig. 8 depicts the soot concentrations in the flame. Whereas the model's predictions were very successful for the heavily sooting Flame_{2,5}, it also predicted substantial soot concentration profiles in the cases of the nearly sooting flames, where no soot was collected experimentally. In reality there was visual evidence of soot in Flame_{1,74} and, particularly, in Flame_{1,83}, see; Fig. 4. However, initial soot inception was observed to occur at the periphery of the flame where lower temperatures favor soot formation [69] and not at the centerline where the sampling probe was placed. Thus, it is likely that sampling for soot at the centerline might have undercut the measurements at the soot onset point. It is also likely that the model overpredicted the magnitude of the soot emissions in these cases, as they were calculated to be only 10-fold lower than those of the highly sooting flame, which does not appear to be commensurate with the visual observations; see Fig. 3. Thus the previously described overprediction of acetylene in the nearly or slightly sooting flames is expected to have contributed significantly to the resulting overpredictions of soot particles. Previous work has shown that in low pressure sooting benzene flames surface growth by acetylene contributed to nearly 70% of the final soot mass [54]. In the same study, the importance of reactions between PAH and their radicals, as well as among such radicals, has been found to be essential for efficient soot nucleation allowing for effective subsequent particle growth. Deliberate omission

of these PAH association reactions, i.e., the description of particle nucleation exclusively by hydrogen abstraction/acetylene addition sequences, resulted in underpredictions by two to three orders of magnitude for particle concentrations and number densities [54]. In the present version of the model, particle nucleation reactions are treated as irreversible, and probably more importantly, rate constants have been based on expressions available for phenyl + benzene and phenyl + phenyl. Activation energies were kept constant, while pre-exponential factors have been scaled corresponding to the collision frequencies [54]. Taking into account the importance of soot nucleation and significantly different temperature profiles in the heavily and nearly sooting flames, inadequate activation energies can have a pronounced effect on predictions of soot formations. For instance, too low activation energies may explain the overpredictions of the resulting soot concentrations.

Further improvements of the model will include a more detailed description of the oxidation of PAH and soot particles of increasing size. There is only limited kinetic information on oxidation reactions and some effort has been made recently to determine oxidation rates for anthracene under certain conditions by our group [70]. Nevertheless, further comprehensive research on this issue is necessary to increase the predictive capability of kinetic models.

A reaction flux analysis has been conducted in the slightly sooting flame ($\phi = 1.83$) in order to gain an understanding of major pathways involved in the consumption of the fuel and its conversion to PAH and finally to soot. For this purpose, rates of production of selected species were determined using a post-processor which is part of the CHEMKIN software package [65]. Consistent with previous findings in the sooting ethylbenzene flame [28], monomolecular decomposition to benzyl ($C_6H_5CH_2$) and methyl radicals was found to be the dominant fuel consumption pathway. Due to the resulting high benzyl concentrations and different from benzene flames where cyclopentadienyl self-combination was the major pathway [52], naphthalene was found to be nearly exclusively formed by reaction of benzyl with propargyl (C_3H_3) radicals [28,71]. Due to its importance as the bottleneck in the reaction sequence leading to PAH of increasing size and ultimately to soot [37,40], the quantitative description of benzene formation has received significant addition and contributions of specific pathways were found to depend significantly on the fuel type and local conditions in the flame [72]. In the present flame, recombination of propargyl radicals [40,72] was found to play a major role in benzene formation, but toluene was identified to be an equally important precursor ($C_7H_8 + H \rightleftharpoons C_6H_6 + CH_3$). Interestingly, decomposition of ethylbenzene by reac-

tion with hydrogen radicals ($C_8H_{10} + H \rightleftharpoons C_6H_6 + C_2H_5$) plays only a secondary role.

Taking into account the importance of styrene (C_8H_8) as product of ethylbenzene [11] and polystyrene [12] decomposition, particularly under pyrolytic conditions, its formation and consumption was investigated in some detail. Monomolecular hydrogen loss from C_8H_9 was found to be the only significant formation pathway. Other possible routes such as the reaction of benzene with vinyl ($C_6H_6 + C_2H_3 \rightleftharpoons C_8H_8 + H$) were found to contribute to its depletion via the reverse reactions. Monomolecular decomposition to benzene and acetylene ($C_8H_8 \rightleftharpoons C_6H_6 + C_2H_2$) is the major styrene consumption pathway, whereas the contribution of this reaction to benzene formation was found to be negligible. However, the pronounced underprediction of styrene by the kinetic model (Fig. 8) may lead to significant underestimation of the role of styrene as benzene precursor. Monomolecular hydrogen loss and hydrogen abstraction by H and OH (in this order) were identified to be formation pathways of C_8H_9 .

Acetylene plays a key role in the growth process of PAH of increasing size and finally soot [37,40,54]. Taking into account the large number of sequential reactions involving acetylene, even relatively small errors in its computed concentrations can have a major impact on final species or soot particle concentrations. Overpredicted soot concentrations in the nearly and slightly sooting flames are likely to be at least partially related to similar overpredictions of acetylene in the postflame zones of these flames (Fig. 8). As for all other investigated species, absolute reaction rates involving acetylene are much smaller in the postflame than in the reaction zone but resulting rates of production can be sufficient to affect species concentrations significantly. Reaction flux analysis of acetylene shows in the postflame zone some continued formation via monomolecular decomposition of C_2H_3 to $C_2H_2 + H$ in addition to oxidative depletion. Oxidation with oxygen radicals to $HCCO + H$ and $HCO + CO$ are by far the most important pathways. Reaction rates depend therefore on the concentrations of O but also to some extent of OH radicals, while H-radical concentrations impact the equilibria of the monomolecular decomposition of C_2H_3 and oxidation to $HCCO + H$. Precise predictions of radical concentrations are challenging and only few experimental data are available in very fuel-rich or even sooting flames. Lack of precision of the kinetic model in the predictions of H, O, and OH radicals may explain, possibly in conjunction with uncertainties of the temperature profile, the overprediction of acetylene in the nearly and slightly sooting ethylbenzene flames investigated in the present work.

6. Conclusions

Combustion-generated species and temperatures were monitored along the axis of three one-dimensional laminar premixed flames of ethylbenzene. The fuel was prevaporized and blended with oxygen and nitrogen gases to generate fuel-rich flames. Experiments were conducted in the vicinity of the soot onset limit. Three flames were examined at equivalence ratios of $\phi = 1.68$ (prior to the visual evidence of soot), $\phi = 1.74$ (perhaps at the very onset), and $\phi = 1.83$ (where luminous streaks of soot were definitely present). Efforts were made to keep the maximum temperature of these flames similar by varying the relative amounts of fuel vapor, oxygen, and diluent (nitrogen). It was thus indicated that the maximum measured flame temperature does not quite uniquely determine the soot onset limit. There was, however, a small spread in temperatures in the postflame region, the effect of which will be investigated further. In the heavily sooting flame of a previous study [28], experimentally observed acetylene concentrations increased along the height above the burner, whereas they decreased in the nearly sooting flames of this study. Also, whereas temperatures in all three nearly sooting flames were similar, significantly lower temperatures were measured throughout the heavily sooting flame. The mole fractions of styrene and phenylacetylene decreased markedly at the onset of soot, which can be observed by comparing mole fractions in Flame_{1.68} with those of both Flame_{1.74} and Flame_{1.83}. Profiles of PAH mole fractions exhibited decreasing trends in Flame_{1.74} and Flame_{1.83}, as incipient soot was generated. Lower-molecular weight PAH (2–3 ring) mole fractions in the nonsooting Flame_{1.68} were higher than those of the slightly sooting flames, whereas the opposite trend was observed for higher-molecular-weight PAH (more than 3-ring PAH). Emissions of carbon monoxide increased with ϕ and generally with distance in the postflame zone. Comparisons of the experimental profiles with predictions of a detailed kinetic model were encouraging, given that the regime of soot inception is definitely challenging. Predictions ranged from excellent in fluorene to fair in phenanthrene to inconsistent in styrene. A reaction flux analysis was conducted and monomolecular decomposition to benzyl and methyl radicals was found to be the dominant fuel consumption pathway. Recombination of propargyl radicals was found to play a major role in benzene formation, but toluene was identified to be an equally important precursor. Naphthalene was found to be nearly exclusively formed by reaction of benzyl with propargyl radicals. Areas of needed improvement have been identified to eventually render the model a comprehensive predictive tool.

Appendix A

Table A.1

Mole fractions of fixed gases, light hydrocarbons, and monocyclic aromatic hydrocarbons for nearly sooting or slightly sooting flames ($\phi = 1.68, 1.74, 1.83$)

Species	Height from the surface of the burner (mm) Flame	1	3	5	7	9
O ₂	$\phi = 1.68$	6.45E-03	6.01E-03	5.66E-03	4.08E-03	3.06E-03
	$\phi = 1.74$	5.74E-03	6.04E-03		5.91E-03	
	$\phi = 1.83$	5.94E-03	4.87E-03		4.88E-03	
CO	$\phi = 1.68$	1.28E-01	1.40E-01	1.63E-01	1.60E-01	1.74E-01
	$\phi = 1.74$	1.43E-01	1.66E-01		1.74E-01	
	$\phi = 1.83$	1.31E-01	1.57E-01		1.73E-01	
CO ₂	$\phi = 1.68$	8.87E-02	8.60E-02	7.58E-02	7.67E-02	7.66E-02
	$\phi = 1.74$	9.22E-02	8.14E-02		7.47E-02	
	$\phi = 1.83$	9.09E-02	6.90E-02		6.30E-02	
Methane	$\phi = 1.68$	1.69E-03	1.19E-03	2.73E-04	4.72E-05	5.28E-05
	$\phi = 1.74$	1.48E-03	1.06E-03		2.02E-04	
	$\phi = 1.83$	7.41E-04	1.83E-03		2.45E-04	
Ethane	$\phi = 1.68$	2.82E-05	1.58E-05	1.28E-06	8.32E-07	N/A
	$\phi = 1.74$	2.12E-05	9.27E-06		5.85E-07	
	$\phi = 1.83$	1.17E-05	7.41E-06		9.02E-07	
Ethylene	$\phi = 1.68$	5.16E-04	2.45E-04	1.13E-04	2.80E-05	1.49E-05
	$\phi = 1.74$	3.93E-04	3.07E-04		4.86E-05	
	$\phi = 1.83$	2.80E-04	2.71E-04		5.94E-05	
Acetylene	$\phi = 1.68$	2.37E-03	1.97E-03	8.75E-04	1.43E-04	5.93E-05
	$\phi = 1.74$	2.93E-03	2.60E-03		3.55E-04	
	$\phi = 1.83$	1.56E-03	4.89E-03		5.60E-04	
Benzene	$\phi = 1.68$	8.81E-06	4.58E-07	2.78E-07	N/A	N/A
	$\phi = 1.74$	1.98E-06	8.94E-07		7.12E-07	
	$\phi = 1.83$	N/A	1.50E-06		N/A	
Toluene	$\phi = 1.68$	1.81E-07	2.50E-07	1.04E-07	1.07E-07	9.11E-08
	$\phi = 1.74$	1.24E-07	9.57E-08		1.54E-07	
	$\phi = 1.83$	N/A	5.34E-07		5.71E-07	
Styrene	$\phi = 1.68$	4.43E-04	2.20E-04	7.27E-06	3.13E-07	9.47E-08
	$\phi = 1.74$	5.36E-06	1.74E-06		7.18E-08	
	$\phi = 1.83$	7.28E-06	1.13E-06		2.62E-06	
Phenylacetylene	$\phi = 1.68$	3.39E-05	2.94E-05	2.26E-07	1.13E-07	1.24E-08
	$\phi = 1.74$	1.94E-06	9.49E-07		N/A	
	$\phi = 1.83$	3.65E-06	3.56E-06		8.92E-08	

Table A.2

Mole fractions of polycyclic aromatic hydrocarbons (PAH) for nearly sooting or slightly sooting flames ($\phi = 1.68, 1.74, 1.83$)

Species	Height from the surface of the burner (mm) Flame	1	3	5	7	9
Indene	$\phi = 1.68$	1.77E-05	1.44E-05	1.00E-07	5.30E-08	3.51E-08
	$\phi = 1.74$	8.45E-06	6.37E-06		N/A	
	$\phi = 1.83$	9.73E-06	4.06E-06		2.39E-08	

(continued on next page)

Table A.2 (continued)

Species	Height from the surface of the burner (mm) Flame	1	3	5	7	9
Naphthalene	$\phi = 1.68$	3.18E-05	2.26E-05	1.42E-06	2.26E-06	8.87E-07
	$\phi = 1.74$	1.89E-05	7.99E-06		1.22E-06	
	$\phi = 1.83$	1.49E-05	9.78E-06		1.04E-06	
Biphenyl	$\phi = 1.68$	5.62E-07	5.46E-07	2.95E-09	2.46E-09	N/A
	$\phi = 1.74$	3.13E-07	1.64E-07		N/A	
	$\phi = 1.83$	3.53E-07	8.03E-08		N/A	
Biphenylene	$\phi = 1.68$	1.55E-08	2.79E-08	2.27E-08	1.25E-08	7.04E-09
	$\phi = 1.74$	9.23E-09	1.49E-08		N/A	
	$\phi = 1.83$	1.85E-08	3.41E-08		N/A	
Fluorene	$\phi = 1.68$	1.21E-06	9.50E-07	2.30E-09	N/A	N/A
	$\phi = 1.74$	7.29E-07	5.61E-07		N/A	
	$\phi = 1.83$	8.02E-07	3.71E-07		N/A	
Acenaphthylene	$\phi = 1.68$	3.93E-06	2.36E-06	5.00E-09	N/A	N/A
	$\phi = 1.74$	5.65E-06	6.33E-06		5.77E-08	
	$\phi = 1.83$	3.96E-06	6.59E-06		1.14E-08	
Phenanthrene	$\phi = 1.68$	3.51E-06	1.52E-06	6.65E-08	2.76E-08	2.68E-08
	$\phi = 1.74$	1.24E-06	1.02E-06		3.72E-10	
	$\phi = 1.83$	8.34E-07	6.45E-07		3.64E-09	
4H-Cyclopenta[def]phenanthrene	$\phi = 1.68$	2.89E-07	1.66E-07	N/A	N/A	N/A
	$\phi = 1.74$	1.65E-07	5.03E-07		4.56E-08	
	$\phi = 1.83$	3.21E-07	3.02E-07		N/A	
Acephenanthrylene	$\phi = 1.68$	7.20E-08	5.83E-08	N/A	N/A	N/A
	$\phi = 1.74$	9.73E-08	1.55E-07		N/A	
	$\phi = 1.83$	5.57E-08	1.49E-07		N/A	
Fluoranthene	$\phi = 1.68$	4.42E-07	1.67E-07	1.27E-07	N/A	N/A
	$\phi = 1.74$	5.35E-07	7.43E-07		N/A	
	$\phi = 1.83$	2.48E-07	5.17E-07		N/A	
Pyrene	$\phi = 1.68$	1.97E-07	1.39E-07	N/A	N/A	N/A
	$\phi = 1.74$	4.47E-07	8.02E-07		N/A	
	$\phi = 1.83$	1.35E-07	8.14E-07		N/A	
Total PAH	$\phi = 1.68$	9.60E-05	8.88E-05	2.46E-05	1.87E-05	1.03E-06
	$\phi = 1.74$	3.85E-05	2.61E-05		1.98E-06	
	$\phi = 1.83$	3.31E-05	2.44E-05		1.47E-06	

Table A.3

Mole fractions of oxygenated polycyclic aromatic compounds (PAC) for nearly sooting or slightly sooting flames ($\phi = 1.68, 1.74, 1.83$)

Species	Height from the surface of the burner (mm) Flame	1	3	5	7	9
Benzaldehyde	$\phi = 1.68$	7.44E-06	2.08E-06	1.26E-07	1.04E-07	9.82E-08
	$\phi = 1.74$	9.27E-07	3.43E-07		1.28E-07	
	$\phi = 1.83$	5.11E-07	4.82E-07		1.66E-07	
Phenol	$\phi = 1.68$	8.38E-06	1.33E-06	5.75E-08	3.60E-08	1.24E-08
	$\phi = 1.74$	1.75E-06	3.37E-07		N/A	
	$\phi = 1.83$	3.74E-06	2.16E-07		N/A	

Table A.3 (continued)

Species	Height from the surface of the burner (mm) Flame	1	3	5	7	9
Benzofuran	$\phi = 1.68$	2.84E-06	1.35E-07	2.51E-08	4.19E-08	N/A
	$\phi = 1.74$	6.32E-07	2.37E-07		N/A	
	$\phi = 1.83$	4.78E-07	9.04E-08		1.08E-08	
2-Naphthalenecarboxaldehyde	$\phi = 1.68$	1.89E-07	8.54E-08	N/A	N/A	N/A
	$\phi = 1.74$	5.91E-09	N/A		N/A	
	$\phi = 1.83$	N/A	6.86E-08		N/A	
Dibenzofuran	$\phi = 1.68$	7.91E-07	1.86E-07	6.98E-10	2.09E-09	N/A
	$\phi = 1.74$	3.04E-07	1.31E-07		N/A	
	$\phi = 1.83$	3.69E-07	5.13E-08		N/A	
Fluorene-9-one	$\phi = 1.68$	2.67E-06	2.75E-07	N/A	N/A	N/A
	$\phi = 1.74$	2.64E-08	7.86E-09		N/A	
	$\phi = 1.83$	8.02E-09	N/A		N/A	
9,10-Anthracenedione	$\phi = 1.68$	6.46E-08	2.18E-07	5.22E-08	3.97E-08	N/A
	$\phi = 1.74$	5.60E-08	5.90E-08		4.64E-08	
	$\phi = 1.83$	3.54E-08	5.24E-08		3.00E-08	

Table A.4

Mole fractions of fixed gases, light hydrocarbons, and monocyclic aromatic hydrocarbons for highly sooting flame ($\phi = 2.5$)

Species	Height from the surface of the burner (mm) Flame	1	3	5	7	9
O ₂	$\phi = 2.5$	4.95E-02	4.52E-02	9.00E-03	1.13E-02	N/A
CO	$\phi = 2.5$	2.02E-01	2.17E-01	2.25E-01	2.38E-01	2.29E-01
CO ₂	$\phi = 2.5$	4.81E-02	5.00E-02	5.88E-02	6.37E-02	4.22E-02
Methane	$\phi = 2.5$	5.04E-03	7.27E-03	9.92E-03	1.02E-02	N/A
Ethane	$\phi = 2.5$	3.59E-05	2.98E-05	2.37E-05	9.08E-06	N/A
Ethylene	$\phi = 2.5$	2.12E-03	2.92E-04	4.28E-04	3.53E-04	1.19E-04
Acetylene	$\phi = 2.5$	3.38E-03	6.09E-03	8.79E-03	1.04E-02	1.62E-02
Benzene	$\phi = 2.5$	6.58E-06	4.10E-06	1.62E-06	9.96E-07	3.39E-07
Toluene	$\phi = 2.5$	2.99E-07	2.42E-07	1.84E-07	1.11E-07	1.22E-07
Styrene	$\phi = 2.5$	1.87E-03	6.36E-04	1.24E-04	3.42E-05	1.27E-06
Phenyl acetylene	$\phi = 2.5$	1.85E-05	2.47E-05	6.51E-05	4.42E-05	1.30E-05

Table A.5

Mole fractions of polycyclic aromatic hydrocarbons (PAH) for highly sooting flame ($\phi = 2.5$)

Species	Height from the surface of the burner (mm) Flame	1	3	5	7	9
Indene	$\phi = 2.5$	5.37E-05	9.05E-05	3.85E-05	2.62E-05	5.31E-06
Naphthalene	$\phi = 2.5$	1.89E-04	3.63E-04	1.94E-04	1.16E-04	2.61E-05
Biphenyl	$\phi = 2.5$	3.69E-05	5.54E-05	1.05E-05	7.95E-06	1.55E-07
Biphenylene	$\phi = 2.5$	1.86E-07	1.84E-07	1.58E-07	1.33E-07	1.18E-07
Fluorene	$\phi = 2.5$	5.63E-06	1.15E-05	8.63E-06	6.72E-06	9.58E-07
Acenaphthylene	$\phi = 2.5$	2.50E-05	5.44E-05	9.42E-05	7.16E-05	3.43E-05
Phenanthrene	$\phi = 2.5$	2.50E-05	4.37E-05	2.69E-05	1.56E-05	2.62E-06

(continued on next page)

Table A.5 (continued)

Species	Height from the surface of the burner (mm) Flame	1	3	5	7	9
4H-Cyclopenta[def]phenanthrene	$\phi = 2.5$	3.66E-07	7.59E-07	1.77E-06	1.23E-06	6.51E-07
Acephenanthrylene	$\phi = 2.5$	3.83E-07	9.34E-07	1.78E-06	2.34E-06	3.06E-07
Fluoranthene	$\phi = 2.5$	1.58E-06	3.33E-06	5.61E-06	3.43E-06	1.14E-06
Pyrene	$\phi = 2.5$	1.04E-06	1.34E-06	6.14E-06	7.00E-06	2.77E-06
Benzo[ghi]fluoranthene	$\phi = 2.5$	2.22E-07	2.55E-07	1.27E-06	8E-07	5.02E-07
Cyclopenta[cd]pyrene	$\phi = 2.5$	2.36E-07	7.82E-07	1.26E-06	8.07E-07	5.04E-07
Benzo[a]pyrene	$\phi = 2.5$	7.14E-08	1.63E-08	4.6E-07	3.95E-07	8.79E-08
Benzo[b]fluoranthene	$\phi = 2.5$	1.05E-07	2.14E-07	3.71E-07	2.54E-07	3.19E-08
Benzo[a]fluorene	$\phi = 2.5$	5.12E-08	1.77E-07	1.51E-07	1.50E-07	6.69E-09
Perylene	$\phi = 2.5$	N/A	3.63E-09	7.40E-08	9.25E-08	8.12E-09
Total PAH	$\phi = 2.5$	4.28E-04	7.05E-04	4.21E-04	2.83E-04	7.76E-05

Table A.6

Mole fractions of oxygenated polycyclic aromatic compounds (PAC) for highly sooting flame ($\phi = 2.5$)

Species	Height from the surface of the burner (mm) Flame	1	3	5	7	9
Benzaldehyde	$\phi = 2.5$	3.07E-04	1.33E-04	1.37E-05	4.84E-06	1.61E-07
Phenol	$\phi = 2.5$	6.77E-04	4.40E-04	2.47E-05	6.93E-06	N/A
Benzofuran	$\phi = 2.5$	1.72E-04	1.16E-04	1.02E-05	6.70E-06	N/A
2-Naphthalenecarboxaldehyde	$\phi = 2.5$	1.74E-06	4.26E-07	1.72E-07	6.80E-08	N/A
Dibenzofuran	$\phi = 2.5$	4.92E-05	6.20E-05	6.86E-06	6.90E-06	N/A
Fluorene-9-one	$\phi = 2.5$	4.62E-06	1.92E-06	8.15E-07	1.35E-06	N/A
9,10-Anthracenedione	$\phi = 2.5$	1.99E-07	1.74E-07	3.73E-08	2.17E-08	N/A

References

- http://www.conocophillips.com/newsroom/other_resources/energyanswers/gasoline.htm.
- <http://www.eia.doe.gov/emeu/steo/pub/contents.html>.
- <http://omrpublic.iea.org>.
- <http://www.eco-usa.net/toxics/ethbenz.shtml>.
- <http://www.westernpetro.com/doc/GasolineMSDS.doc>.
- <http://www.uni-tuebingen.de/zag/hydrogeochemistry/download/SayoOxygenGasoline.pdf>.
- <http://www.vdh.state.va.us/HHControl/peetrofac.PDF>.
- J.C. Street, A. Thomas, *Fuel* 34 (1955) 4.
- D.B. Olson, J.C. Pickens, *Combust. Flame* 57 (1984) 199–208.
- J.L. Durant, W.F. Busby, A.L. Lafleur, B.W. Penman, C.L. Crespi, *Mutation Res.* 371 (1996) 123–157.
- C. Venkat, K. Brezinsky, I. Glassman, *Proc. Combust. Inst.* 19 (1982) 143–152.
- W. Klusmeier, K.H. Ohrbach, A. Ketrup, *Thermochim. Acta* 103 (1986) 231–237.
- T. Panagiotou, Y.A. Levendis, J. Carlson, P. Vouros, *Proc. Combust. Inst.* 26 (1996) 2421–2430.
- T. Panagiotou, Y.A. Levendis, *Combust. Sci. Technol.* 137 (1998) 121–147.
- B.E. Shemwell, Y.A. Levendis, *J. Air Waste Manage. Assoc.* 50 (2000) 94–102.
- B. Shemwell, Y.A. Levendis, *J. Air Waste Manage. Assoc.* 50 (2000) 2421–2430.
- T. Panagiotou, Y.A. Levendis, *Combust. Flame* 99 (1994) 53–74.
- T. Panagiotou, Y.A. Levendis, M.A. Delichatsios, *Combust. Sci. Technol.* 103 (1994) 63–84.
- T. Panagiotou, Y.A. Levendis, J.B. Carlson, Y.M. Dunayevskiy, P. Vouros, *Combust. Sci. Technol.* 116–117 (1996) 91–128.
- L. Wheatley, Y.A. Levendis, P. Vouros, *Environ. Sci. Technol.* 27 (1993) 2885–2895.
- B. Courtemanche, Y.A. Levendis, *Fuel* 77 (1998) 183–196.
- J. Wang, Y.A. Levendis, H. Richter, J.B. Howard, J. Carlson, *Environ. Sci. Technol.* 35 (2001) 3541–3552.
- J. Wang, H. Richter, Y.A. Levendis, J.B. Howard, J. Carlson, *Environ. Sci. Technol.* 36 (2002) 797–808.
- J. Wang, G. Ferreiro, H. Richter, J.B. Howard, Y.A. Levendis, J. Carlson, *Proc. Combust. Inst.* 28 (2002) 2477–2484.
- Z. Wang, J. Wang, H. Richter, J.B. Howard, J. Carlson, Y.A. Levendis, *Energy Fuels* 17 (2003) 999–1013.
- Z. Wang, H. Richter, J.B. Howard, J. Carlson, Y.A. Levendis, *Ind. Eng. Chem. Res.* 43 (2004) 2873–2886.
- C. Westblad, Y.A. Levendis, H. Richter, J.B. Howard, J. Carlson, *Chemosphere* 49 (2002) 395–412.

- [28] A. Ergut, S. Granata, J. Jordan, J. Carlson, J.B. Howard, H. Richter, Y.A. Levendis, *Combust. Flame* 144 (2006) 757–772.
- [29] S.K. Durlak, P. Biswas, J. Shi, M.J. Bernhard, *Environ. Sci. Technol.* 32 (1998) 2301–2307.
- [30] F. Takahashi, I. Glassman, *Combust. Sci. Technol.* 37 (1984) 1.
- [31] S.C. Graham, J.B. Homer, J.L.J. Rosenfeld, *Proc. R. Soc. London Ser. A* 344 (1975) 259–285.
- [32] C.A. Amann, D.C. Siegl, *Aerosol Sci. Technol.* 1 (1982) 73–101.
- [33] J.B. Heywood, *Internal Combustion Engine Fundamentals*, McGraw–Hill, New York, 1988.
- [34] P. Markatou, H. Wang, M. Frenklach, *Combust. Flame* 93 (1993) 467.
- [35] P.B. Sunderland, D.L. Urban, D.P. Stocker, B.H. Chao, R.L. Axelbaum, *Combust. Sci. Technol.* 176 (2004) 2143–2164.
- [36] C.S. McEnally, L.D. Pfefferle, B. Atakan, K. Kohse-Hoinghaus, *Prog. Energy Combust. Sci.* 32 (2006) 247–294.
- [37] M. Frenklach, *Phys. Chem. Chem. Phys.* 4 (2002) 2028–2037.
- [38] I. Glassman, *Proc. Combust. Inst.* 22 (1988) 295–311.
- [39] J.A. Miller, C.F. Melius, *Combust. Flame* 91 (1992) 21.
- [40] H. Richter, J.B. Howard, *Prog. Energy Combust. Sci.* 26 (2000) 565–608.
- [41] A. D’Anna, A. Violi, *Energy Fuels* 19 (2005) 79–86.
- [42] A. D’Anna, A. Violi, A. D’Alessio, A.F. Sarofim, *Combust. Flame* 127 (2001) 1995–2003.
- [43] H.F. Calcote, D.M. Manos, *Combust. Flame* 49 (1983) 289–304.
- [44] P.M. Hanson, D.H. Rouvray, *J. Phys. Chem.* 91 (1987) 2981.
- [45] R.C. Millikan, *J. Phys. Chem.* 66 (1962) 794.
- [46] W.E. Kaskan, *Proc. Combust. Inst.* 6 (1956) 134–143.
- [47] H.F. Calcote, D.B. Olson, *Combust. Sci. Technol.* 28 (1982) 315.
- [48] D.B. Olson, S. Madronich, *Combust. Flame* 60 (1985) 203–213.
- [49] H. Böhm, D. Hesse, H. Jander, B. Luers, J. Pietscher, H.G.G. Wagner, M. Weiss, *Proc. Combust. Inst.* 22 (1988) 403–411.
- [50] F. Kurlbaum, *Phys. Z.* (Feb. 1, 1902) 187.
- [51] M.M. Harris, G.B. King, N.M. Laurendeau, *Combust. Flame* 64 (1986) 99–112.
- [52] H. Richter, T.G. Benish, O.A. Mazyar, W.H. Green, J.B. Howard, *Proc. Combust. Inst.* 28 (2000) 2609–2618.
- [53] A. Gomez, M.G. Littman, I. Glassman, *Combust. Flame* 70 (1987) 225–241.
- [54] H. Richter, S. Granata, W.H. Green, J.B. Howard, *Proc. Combust. Inst.* 30 (2005) 1397–1405.
- [55] J.T. McKinnon, Ph.D. thesis, Massachusetts Institute of Technology, Cambridge, MA, 1989.
- [56] A. Ergut, Y. Levendis, in: *Proc. of ASME International Mechanical Eng. Congress and Expo. (IMECE2005)*, Orlando, FL, 2005.
- [57] K.C. Lin, G.M. Faeth, *Combust. Flame* 115 (1998) 468–480.
- [58] E.L. Nichols, *Phys. Rev.* 10 (1900) 234.
- [59] C.S. McEnally, U.O. Koylu, L.D. Pfefferle, D.E. Rosner, *Combust. Flame* 109 (1997) 701–720.
- [60] W.C. Reynolds, STANJAN Multicomponent Equilibrium Program v. 3.60, 1986.
- [61] C.J. Pope, J.B. Howard, *Aerosol Sci. Technol.* 27 (1997) 73–94.
- [62] J. Yu, R. Sumathi, W.H. Green, *J. Am. Chem. Soc.* 126 (2004) 12685–12700.
- [63] W.J. Grieco, A.L. Lafleur, K.C. Swallow, H. Richter, K. Taghizadeh, J.B. Howard, *Proc. Combust. Inst.* 27 (1998) 1669–1675.
- [64] J.D. Bittner, J.B. Howard, *Proc. Combust. Inst.* 18 (1981) 1105–1116.
- [65] R.J. Kee, F.M. Rupley, J.A. Miller, M.E. Coltrin, J.F. Grcar, E. Meeks, H.K. Moffat, A.E. Lutz, G. Dixon-Lewis, M.D. Smooke, J. Warnatz, G.H. Evans, R.S. Larson, R.E. Mitchell, L.R. Petzold, W.C. Reynolds, M. Caracotsios, W.E. Stewart, P. Glarborg, C. Wang, C.L. McLellan, O. Adigun, W.G. Houf, C.P. Chou, S.F. Miller, P. Ho, P.D. Young, D.J. Young, *CHEMKIN Release, 4.0.2*, Reaction Design, San Diego, CA, 2005.
- [66] A.Y. Chang, J.W. Bozzelli, A.M. Dean, *Z. Phys. Chem.* 214 (2000) 1533–1568.
- [67] A. Burcat, Third Millennium Ideal Gas and Condensed Phase Thermochemical Database for Combustion, Report #867, Technion Aerospace Engineering (TAE), 2001; <ftp://ftp.technion.ac.il/pub/supported/aetdd/thermodynamics/>.
- [68] E.R. Ritter, J.W. Bozzelli, *Int. J. Chem. Kinet.* 23 (1991) 767–778.
- [69] M. Bachmann, W. Wiese, K.-H. Homann, *Combust. Flame* 101 (1995) 548–550.
- [70] J. DeCoster, A. Ergut, Y. Levendis, H. Richter, J.B. Howard, J.B. Carlson, *Proc. Combust. Inst.* 31 (2007) 491–499.
- [71] A. D’Anna, A. Violi, *Proc. Combust. Inst.* 27 (1998) 425–433.
- [72] H. Richter, J.B. Howard, *Phys. Chem. Chem. Phys.* 4 (2002) 2038–2055.